J Mater Sci (2017) 52:3687–3696

Batteries and Supercapacitors

Manganese dioxide–carbon nanotube composite electrodes with high active mass loading for electrochemical supercapacitors

C. Wallar[1], D. Luo[1], R. Poon[1], and I. Zhitomirsky[1,*]

[1] *Department of Materials Science and Engineering, McMaster University, 1280 Main Street West, Hamilton, ON L8S 4L7, Canada*

Received: 26 September 2016
Accepted: 20 December 2016
Published online: 30 December 2016

ABSTRACT

MnO_2–multiwalled carbon nanotube (MWCNT) composites were prepared for application in supercapacitor electrodes and devices. Good dispersion and mixing of the individual components were achieved using conceptually new strategies, allowing for significant improvement in the electrochemical charge storage properties. Composite C1 was prepared using chelating polyaromatic sulfasalazine molecules, which adsorbed on the individual components, allowed for their good dispersion and improved mixing by creating links between the components. Composite C2 utilized a Schiff base linkage mechanism for improved mixing between MnO_2 and MWCNT. New electrochemical strategies allowed for high capacitance and good capacitance retention at high charge–discharge rates at high active mass loading, which was 30 mg cm^{-2}. Composites C1 and C2 showed capacitances of 4.5 and 4.4 F cm^{-2}, respectively, at a scan rate of 2 mV s^{-1}. However, composite C2 showed a higher capacitance retention at high scan rates, which was found to be 66% at a scan rate of 100 mV s^{-1}. The asymmetric devices, prepared using composite C2 as positive electrodes and activated carbon–carbon black negative electrodes, showed promising performance in a voltage window of 1.6 V.

Introduction

MnO_2 is a promising charge storage material for positive electrodes of electrochemical supercapacitors. The interest in application of MnO_2 for supercapacitors [1–4] results from high theoretical specific capacitance (1370 F g^{-1}) of this material, which exhibits nearly ideal box shape cyclic voltammograms (CVs) in a voltage window of ~0.9 V in mild aqueous electrolytes. The charging mechanism of MnO_2 is given by the reaction [1]:

$$MnO_2 + A^+ + e^- \leftrightarrow MnO_2A, \quad (1)$$

where $A^+ = H^+, Na^+, K^+$. Small particle size and electrode porosity are important for good access of the electrolyte ions (A^+) to the capacitive MnO_2 material. Advanced electrode design methods have been developed in order to facilitate ion diffusion in MnO_2 electrodes [5]. However, the electronic conductivity of MnO_2

Address correspondence to E-mail: zhitom@mcmaster.ca

DOI 10.1007/s10853-016-0711-0

is low, requiring MnO_2 be mixed with conductive additives [6–9]. The reduction of gravimetric capacitance with increasing electrode mass and charge–discharge rate is a major drawback, limiting the use of MnO_2 in supercapacitors. At low charge–discharge rates, the gravimetric capacitance decreased by an order of magnitude with increasing electrode mass [5, 8, 10–12] due to low electronic conductivity and poor electrolyte access to the active material. Recent studies highlighted the importance of the fabrication of composites with high active mass loadings [13]. It has been pointed out [13] that in order to store a useful amount of energy for practical applications, high active mass loadings above 10 mg cm^{-2} are necessary. The challenge researchers now face is to increase the mass loading of the MnO_2 composites while maintaining high gravimetric capacitance. This will lead to high areal capacitance and useful energy density. Significant improvement has been was achieved through the use of carbon nanotubes as conductive additives due to their high conductivity and low percolation limit [8, 12, 14, 15].

Another major challenge in the development of MnO_2-based composite electrodes is the efficient mixing of MnO_2 and conductive additives. This problem was addressed by the use of a redox reaction [16–23] of $KMnO_4$ and carbon materials, which promoted the synthesis of MnO_2 nanoparticles on the surface of carbon nanotubes or graphene:

$$4KMnO_4 + 3C + H_2O \rightarrow 4MnO_2 + K_2CO_3 + 2KHCO_3. \quad (2)$$

In this approach, carbon materials are used as sacrificial reducing agents for the synthesis of MnO_2. The disadvantage of this method is related the degradation of the carbon material structure and properties in the reaction (2) and poor control of composition of the final product. Cathodic and anodic electrodeposition techniques have been developed [5, 24] for the deposition of MnO_2. However, such techniques usually allow for relatively low active mass loadings. An alternative approach is therefore needed to synthesize MnO_2-based composite structures with good mixing of MnO_2 and conductive additives. Colloidal processing is a useful strategy for the fabrication of advanced nanocomposites. Many investigations have been focused on the fabrication of MnO_2 nanoparticles, nanorods, and nanowires [5, 25, 26] for colloidal processing of MnO_2–carbon nanotube composites. However, colloidal methods require the development of efficient dispersants for the individual components.

The need for efficient MnO_2 dispersion has driven the discovery and development of advanced dispersants with chelating properties [27]. These dispersants adsorb strongly on MnO_2 particles due to the creation of chelating bonding to Mn atoms on the particle surface. Various dispersants have been investigated for the dispersion of carbon nanotubes [6, 28–31]. Bile acids are among the most intriguing dispersants for carbon nanotubes [28–31] due to their unique adsorption mechanism, small size, and efficient dispersion. Aromatic chelating co-dispersants have been developed for co-dispersion of MnO_2 and carbon nanotubes [27]. The use of aromatic co-dispersant allowed for relatively high areal capacitance at low scan rates [6]. However, the capacitance still decreased with increasing scan rate.

Despite the significant progresses in the fabrication of MnO_2–carbon nanotube electrodes, further development of advanced techniques for improved dispersion and mixing of individual components is required. It is suggested that further progress in this area will result in advanced electrodes with high areal capacitance and improved capacitance retention at high charge–discharge rates.

The goal of our investigation was the development of new methods for the fabrication of MnO_2–multiwalled carbon nanotube (MWCNT) composite electrodes with improved dispersion and mixing of the individual components. We focused our efforts on fabricating electrodes with high, practically useful mass loadings. One strategy was based on the use of a co-dispersant for MnO_2 and MWCNT, which allowed improved mixing by linking of the individual components. In another method, two different dispersants with selective adsorption on the individual components were used. Improved mixing was achieved by Schiff base formation, which involved the bonding of the individual dispersants that were adsorbed on MnO_2 or MWCNT. Testing results of individual electrodes and devices showed enhanced areal capacitance and good capacitance retention at high charge–discharge rates.

Experimental procedures

Sulfasalazine (SSZ), New Fuchsin (NF), 3,4-Dihydroxybenzaldehyde (DHB), Na_2SO_4 (Aldrich, USA), and MWCNT (ID 4 nm, OD 13 nm, length 1–2 μm, Bayer, Germany) were used as starting materials.

MnO_2 nanoparticles with average size of 50 nm were prepared using the method described in a previous work [32]. Ni foams with 95% porosity were provided by Vale Company.

Suspension S1, containing 4 g L^{-1} MnO_2 and 0.5 g L^{-1} SSZ, and suspension S2, containing 1 g L^{-1} MWCNT and 0.5 g L^{-1} SSZ, in a mixed ethanol–water (50% ethanol) solvent were ultrasonicated and mixed, and the obtained mixture was ultrasonicated again. After filtration, the MnO_2–MWCNT material was washed with water and ethanol, and then dried in air. This material was designated composite C1.

Aqueous suspension S3, containing 4 g L^{-1} MnO_2 and 0.5 g L^{-1} DHB, and suspension S4, containing 1 g L^{-1} MWCNT and 0.5 g L^{-1} NF, were ultrasonicated and mixed, and the obtained mixture was ultrasonicated again. After filtration, the MnO_2–MWCNT material was washed with water and ethanol, and then dried in air. This material was designated composite C2.

Composite MnO_2–MWCNT powders were used for the fabrication of slurries in ethanol for the impregnation of Ni foam current collectors and fabrication of electrodes with active mass loading of 30 mg cm^{-2}.

X-ray diffraction (XRD) studies were performed using a powder diffractometer (Nicolet I2, monochromatized CuKα radiation). The composite materials were analyzed by scanning electron microscopy (SEM) using a JEOL microscope JSM-7000F. FTIR spectroscopy (Bio-Rad, spectrometer FTS-40) was used for the characterization of the materials. For the preparation of samples for the FTIR studies, the suspensions were filtrated and the obtained materials were washed with water and dried in air. Cyclic voltammetry (CV) and impedance spectroscopy investigations were performed using a potentiostat (PARSTAT 2273, Princeton Applied Research, USA). Capacitive behavior of the electrodes was studied in three-electrode cells using 0.5 M Na_2SO_4 aqueous solutions. The area of the working electrode was 1 cm^2. The counter electrode was a platinum gauze, and the reference electrode was a standard calomel electrode (SCE). CV studies were performed at scan rates of 2–100 mV s^{-1}. The integral capacitance $C_s = Q/\Delta VS$ was calculated using half the integrated area of the CV curve to obtain the charge Q, and subsequently dividing the charge Q by the width of the potential window ΔV and electrode area S. The alternating current measurements of complex impedance $Z^* = Z' - iZ''$ were performed in the frequency range of 10 mHz to 100 kHz at the amplitude of the signal of 5 mV. The complex differential capacitance $C_S^* = C_S' - i\,C_S''$ was calculated [33] from the impedance data as $C_S' = Z''/\omega|Z|^2S$ and $C_S'' = Z'/\omega|Z|^2S$, where $\omega = 2\pi f$ (f-frequency). MnO_2–MWCNT positive electrodes were combined with activated carbon–carbon black (AC–CB) negative electrodes for the fabrication of asymmetric cells, which offer an advantage of enlarged voltage window in aqueous solutions. AC–CB electrodes were prepared as was described in a previous investigation [34].

MnO_2–MWCNT and AC–CB electrodes, separated by a porous polyethylene membrane (average pore size of 0.4 μm), were used for the fabrication of asymmetric cells. Aqueous 0.5 M Na_2SO_4 solution was used as an electrolyte. The charge–discharge behavior of the cells was investigated using battery analyzers BST8-MA and BST8-3 (MTI corporation, USA) at currents of 3–50 mA.

Results and discussion

X-ray diffraction patterns of the composites, prepared without additives, and composites C1 and C2 showed small peaks of the birnessite phase of MnO_2 (Supporting information, Figs. S1–S3). However, the composites contained a significant amount of an amorphous MnO_2 phase. The SEM studies (Supporting information, Fig. S4) of the composites, prepared without additives, showed poor mixing of the individual components. Such composites contained large agglomerates of MWCNT and MnO_2. The composites C1 and C2 showed improved mixing of MnO_2 and MWCNT and significant reduction in agglomeration and segregation of the individual components (Supporting information, Figs. S5, S6).

The unique chemical structure (Fig. 1A) and redox properties [35] of SSZ make this material a promising additive for the fabrication of MnO_2–MWCNT electrodes with good dispersion and mixing of the individual components and improved capacitive behavior. SSZ is an anionic polyaromatic molecule, containing a salicylate group. Previous investigations [27] showed strong chelating bonding of salicylate molecules to the surface of inorganic oxides. The adsorbed salicylates provided dispersion of the particles in suspensions. Therefore, a similar mechanism

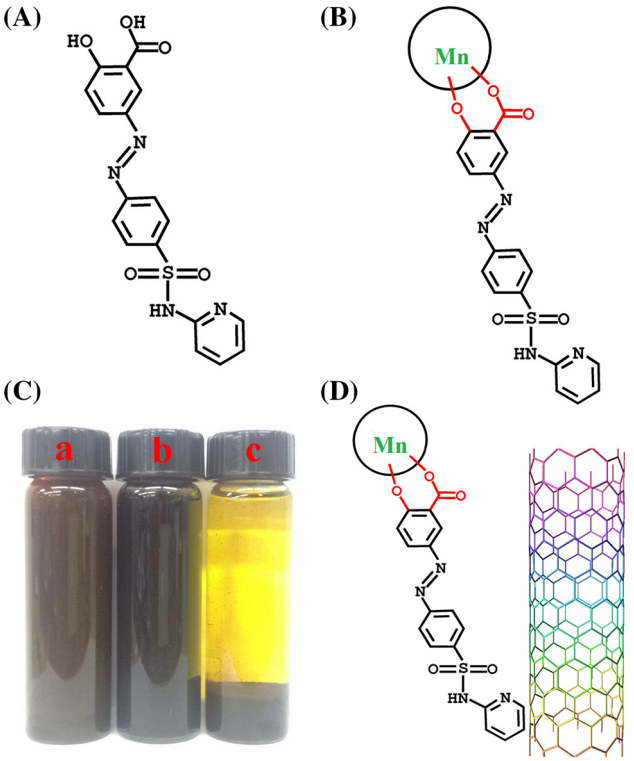

Figure 1 **A** Chemical structure of SSZ. **B** SSZ adsorption on MnO_2, involving complexation of Mn atom on the MnO_2 surface with salicylate group of SSZ. **C** (*a*) suspension S1, (*b*) suspension S2, (*c*) mixture of suspensions S1 and S2. **D** Adsorption of SSZ on MnO_2 and MWCNT.

can result in SSZ adsorption on MnO_2 particles (Fig. 1B). We found that the adsorption of SSZ on MnO_2 resulted in electrosteric dispersion and allowed for the fabrication of stable suspensions [Fig. 1C(a)]. The polyaromatic structure of SSZ makes this material promising for electrosteric dispersion of MWCNT. The adsorption of polyaromatic molecules on MWCNT involves π–π interactions [27]. The addition of SSZ to MWCNT allowed the formation of stable suspensions [Fig. 1C(b)]. However, mixing of the suspension S1 and S2 resulted in rapid precipitation [Fig. 1C(c)]. It is suggested that adsorbed SSZ created links (Fig. 1D) between the MnO_2 particles and MWCNT, because different groups of SSZ showed specific adsorption on different materials. The link formation resulted in improved mixing and the formation of mixed agglomerates, which precipitated due to their larger size.

The FTIR spectrum Fig. 2a of the MnO_2 powder, containing adsorbed SSZ, showed absorptions at 1631, 1531, and 1415 cm^{-1}, related to C–C stretching vibrations of the aromatic rings of SSZ. The

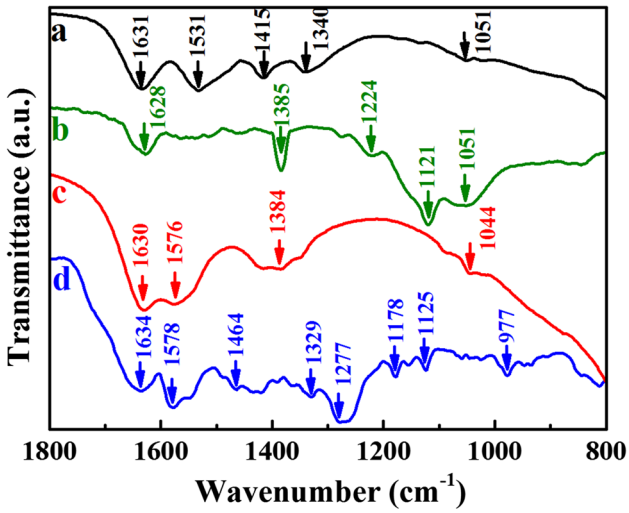

Figure 2 FTIR spectra of *a* MnO_2, containing adsorbed SSZ; *b* composite C1; *c* MnO_2, containing adsorbed DHB; *d* composite C2.

absorption at 1340 cm^{-1} resulted from C=O vibrations of the carboxylic group of SSZ [36]. The FTIR spectrum of the composite C1 Fig. 2b showed a broad absorption at 1628 cm^{-1}, attributed to C–C stretching vibrations of aromatic rings of SSZ. The stretching vibration of surface carboxyl groups of MWCNT [36, 37] and C–O vibrations [38] of SSZ contributed to absorption at 1385 and 1224 cm^{-1}, respectively. The absorptions at 1121 and 1051 cm^{-1} resulted from bending C–H vibrations [38] of SSZ. Therefore, the results of the FTIR studies confirmed that composite C1 contained adsorbed SSZ.

Electrochemical testing results showed improved capacitive behavior of the composite C1, compared to the composite material, prepared without SSZ. The comparison of the CVs at different scan rates, shown in Fig. 3A, B revealed larger CV areas of the electrodes, prepared using composite C1. The larger CV areas indicated higher capacitance (Fig. 3C). The electrode, prepared using composite C1 showed a capacitance of 4.5 F cm^{-2} at a scan rate of 2 mV s^{-1}. The capacitance retention at a scan rate of 100 mV s^{-1} was 36%. Figure 4A compares electrochemical impedance data presented in the Nyquist plot. The electrodes, prepared using composite C1, showed significantly lower resistance $R = Z'$, compared to the composite without dispersant. The lower Z'' values for the composite C1 resulted from higher capacitance. The frequency dependences of the components of complex impedance (Fig. 4B, C) showed a relaxation-type behavior [39], as indicated

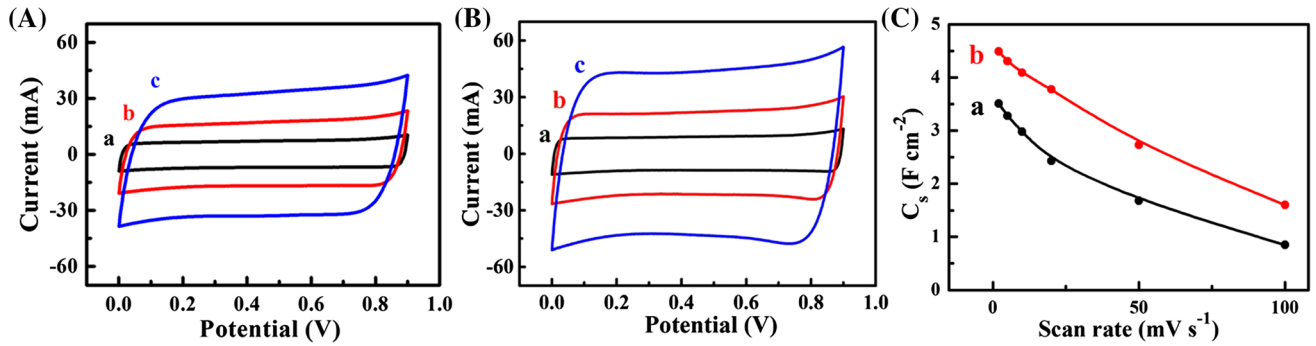

Figure 3 **A**, **B** CVs at scan rates of *a* 2, *b* 5 and *c* 10 mV s^{-1} for **A** MnO_2–MWCNT composite, prepared without additives. B) Composite C1. **C** Capacitance versus scan rate for *a* MnO_2–MWCNT composite prepared without additives, *b* composite C1.

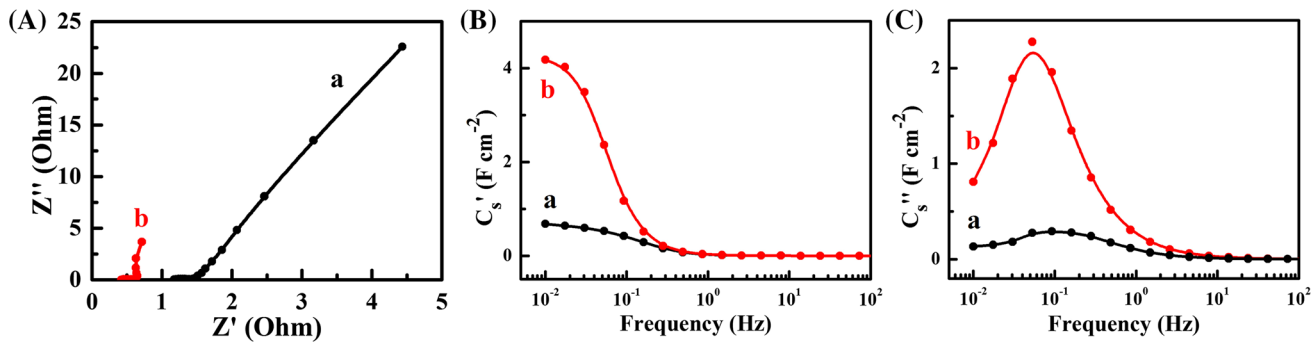

Figure 4 **A** Nyquist plot of complex impedance. **B**, **C** Frequency dependencies of **B** C'_S and **C** C''_S, calculated from the impedance data for *a* MnO_2–MWCNT composite prepared without additives and *b* composite C1.

by the reduction of C'_S with increasing frequency and corresponding maximum in C''_S. The composite C1 showed significantly higher C'_S, compared to the composite, prepared without dispersant. The low frequency values of capacitance C'_S of the composite C1, obtained from the impedance data, are comparable with C_S values derived from the CV data at low scan rates. The higher capacitances, obtained from the CV and impedance data and lower resistance, are attributed to improved dispersion and mixing achieved using SSZ. However, we cannot exclude a possibility that redox behavior [35] of SSZ contributed to enhanced capacitance of composite C1.

In this investigation, we have developed another strategy for the fabrication of MnO_2–MWCNT composites with improved dispersion and mixing of individual components. The approach is based on the use of different dispersants for MnO_2 and MWCNT with selective adsorption on the individual components. A Schiff base linkage mechanism has been utilized for the improved mixing of MnO_2 and MWCNT.

Previous investigation showed that organic dyes such as pyrocatechol violet [40], crystal violet [41], and other isostructural dyes [42, 43] exhibited strong adsorption on MWCNT and allowed for efficient dispersion. The chemical structure of the dyes was beneficial for their adsorption on MWCNT. We found that NF, which has a similar aromatic structure (Fig. 5A), adsorbed on MWCNT and allowed for good MWCNT dispersion.

It is known that stable Schiff bases are formed by fuchsin reactions with aldehydes [44–46]. The following reaction [44] occurs in solutions of fuchsin (F–NH_2) and aldehyde (R–COH):

$$F{-}NH_2 + R{-}COH \rightarrow F{-}N = CHR + H_2O. \quad (3)$$

A Schiff base linkage mechanism has been utilized in many investigations for the formation of aerogels [47, 48], surface modification of materials [49, 50], and other applications [44–46, 51]. Figure 5B shows a chemical structure of an aldehyde-type DHB molecule, which was selected in our investigation for the surface modification of MnO_2. The chemical structure of DHB includes a catechol ligand, which is a powerful complexing agent. Previous investigations [27] showed that molecules from the catechol family strongly adsorbed

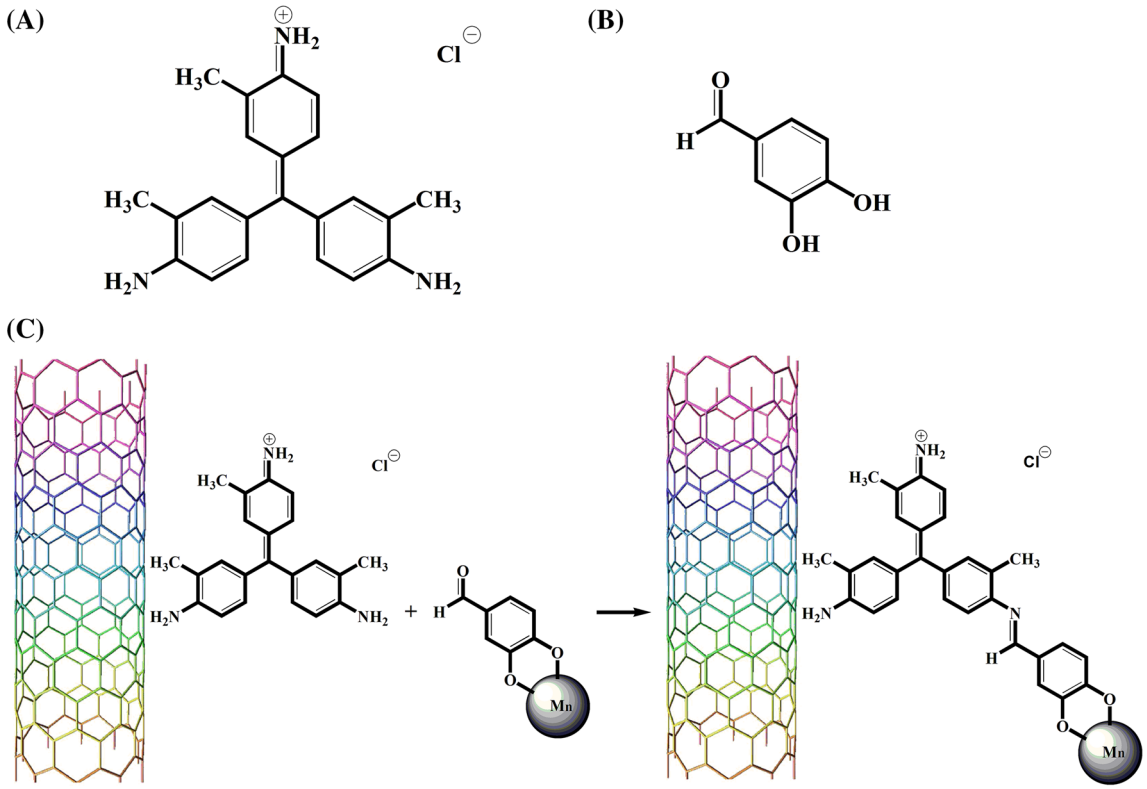

Figure 5 **A**, **B** Chemical structures of **A** NF and **A** DHB; and **C** chemical reaction of NF, adsorbed on MWCNT and DHB, adsorbed on MnO_2.

on the surface of oxide particles by creating catecholate-type bonds with metal atoms on the particle surface. Various molecules from the catechol family were used as efficient dispersing agents for the dispersion of various materials [27]. The adsorbed molecules facilitated charge transfer at the organic–inorganic interface [27]. MnO_2 particles were dispersed in water using DHB and then mixed with MWCNT suspensions, containing NF for the fabrication of composite C2 in the Schiff base reaction (Fig. 5C).

The FTIR spectrum of the MnO_2 powder, containing adsorbed DHB (Fig. 2c), showed absorptions at 1630 and 1576 cm^{-1}, attributed to C–C vibrations of the aromatic ring [36] of DHB. The broad absorption around 1384 cm^{-1} resulted from the C–C vibrations of the aromatic ring and C=O vibrations of DHB [36]. C–H vibrations [38] of DHB contributed to absorption at 1044 cm^{-1}. The FTIR spectrum of composite C2 is presented in Fig. 2d. The absorptions at 1634, 1578, and 1464 cm^{-1} are attributed to C–C stretching vibrations of aromatic rings [52] of the Schiff base. Moreover, the –C=N– stretching vibrations [49] contributed to the broad peak centered at 1634 cm^{-1}. The C–O vibrations [53, 54] contributed to the adsorption at 1329 and 1277 cm^{-1}. Bending C–H vibrations [38] resulted in absorptions at 1178, 1125, and 977 cm^{-1}. The FTIR results indicated that composite C2 contained adsorbed Schiff base.

Figure 6 shows CV data at different scan rates and capacitance versus scan rate dependence for the composite C2. The CV data showed good capacitive behavior in a voltage window of 0.9 V. The capacitance at 2 mV s^{-1} was 4.4 F cm^{-2}. The electrodes showed a remarkable capacitance of 2.9 F cm^{-2} at a scan rate of 100 mV s^{-1} and a capacitance retention (Fig. 6) of 66%. The capacitance of electrodes usually decreases with increasing scan rates due to poor composite conductivity. The higher capacitance at 100 mV s^{-1} and improved capacitance retention of composite C2, compared to composite C1, resulted from better dispersion and mixing of the individual components. Moreover, composite C2 showed (Fig. 7A) lower resistance $R = Z'$, and the slope of the Nyquist plot was close to 90°, indicating good capacitive behavior. The relaxation-type dispersion of the complex capacitance shifted to higher frequencies (Fig. 7B, C) for composite C2, compared to composite C1. This result is in agreement with CV data,

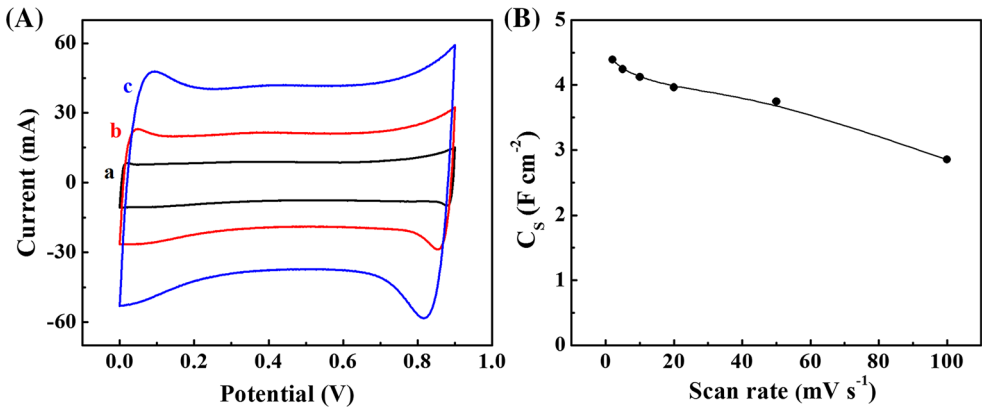

Figure 6 **A** CVs at scan rates of *a* 2, *b* 5 and *c* 10 mV s^{-1}. **B** Capacitance versus scan rate for composite C2.

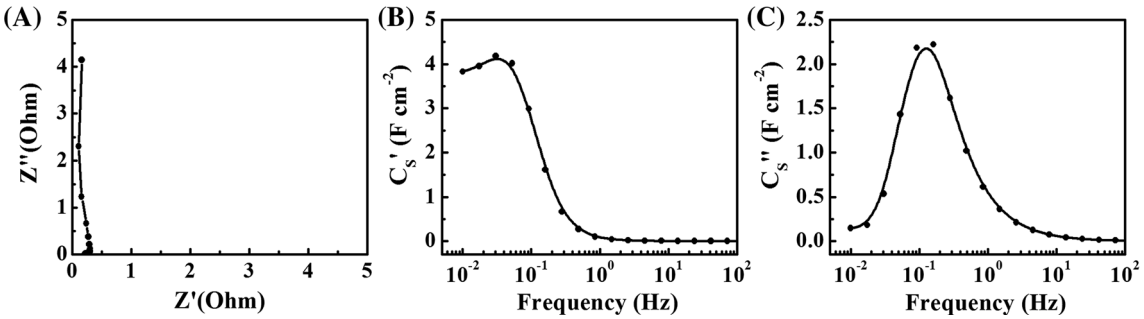

Figure 7 **A** Nyquist plot of complex impedance. **B**, **C** Frequency dependencies of **B** C_S', **C** C_S'', calculated from the impedance data for composite C2.

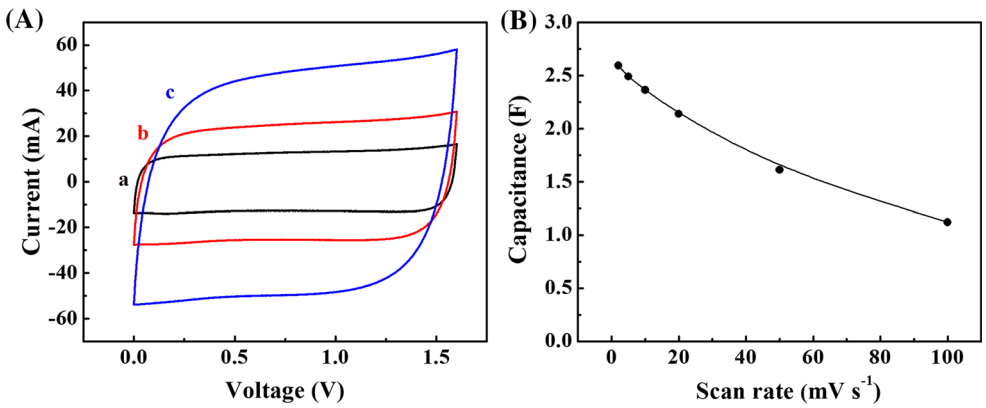

Figure 8 **A** CVs at scan rates of *a* 5, *b* 10 and *c* 20 mV s^{-1}. **B** Capacitance versus scan rate for an asymmetric device, containing composite C2 as a positive electrode and AC–CB as a negative electrode.

indicating better capacitance retention of the composite C2 at high scan rates. The electrodes, containing composite C2 as an active material, showed a capacitance retention of 83% after 5000 cycles (Supporting information, Fig.S7). The C2 electrodes with active mass of 30 mg cm^{-2}, prepared using Schiff base linkage mechanism, showed significantly higher areal capacitance at 100 mV s^{-1}, compared to the electrodes with mass loadings of 40 mg cm^{-2}, prepared using co-dispersants for MnO_2 and MWCNT [6] and by the electrostatic heterocoagulation method [36].

The composite C2 electrodes were combined with the AC–CB electrode for the fabrication of asymmetric devices. The obtained cells showed nearly box shape CVs (Fig. 8A) in a voltage window of 1.6 V. The box shape CVs and increase in current with increasing scan rate indicated good capacitive behavior. The asymmetric device with total active mass of positive and negative electrodes of 152 mg

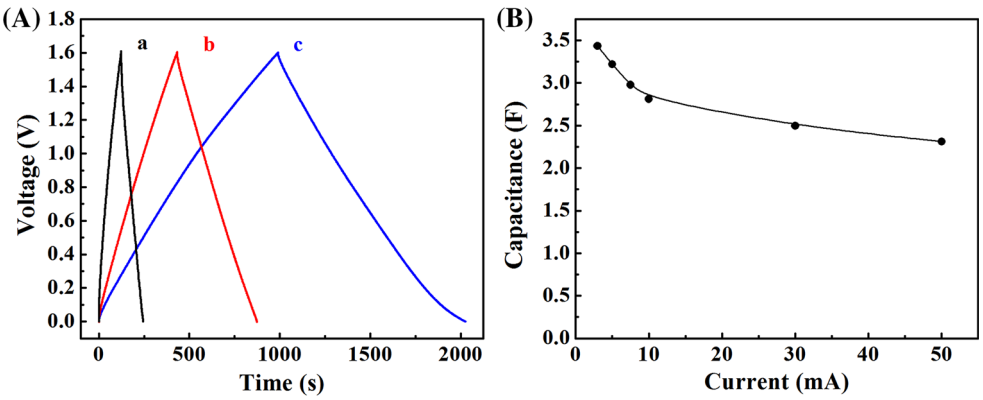

Figure 9 **A** Charge–discharge behavior at currents of *a* 30, *b* 10, *c* 5 mA. **B** Capacitance versus discharge current for an asymmetric device, containing composite C2 as a positive electrode and AC–CB as a negative electrode.

showed (Fig. 8B) a capacitance of 2.59 F at a scan rate of 2 mV s^{-1} and capacitance retention of 43% at a scan rate of 100 mV s^{-1}. The galvanostatic charge–discharge curves (Fig. 9A) were of symmetric triangular shape in a voltage window of 1.6 V. The capacitance, calculated from the discharge data (Fig. 9B), decreased from 3.43 to 2.31 F with increasing discharge current from 3 to 50 mA.

Conclusions

Two strategies have been developed for the fabrication of MnO_2–MWCNT electrodes, based on the use of advanced dispersants, which allowed for improved mixing of the individual components. The salicylate and catechol groups of the dispersants allowed for their strong adsorption on MnO_2 by creation of chelating bonds with Mn atoms on the particle surface. The π–π interactions governed the dispersant adsorption on MWCNT. The SSZ dispersant, used for the fabrication of composite C1, allowed for improved mixing by creating links between MnO_2 and MWCNT. In another strategy, the Schiff base linkage mechanism allowed for improved mixing of the components in the composite C2. Electrochemical testing results showed improved performance of composites C1 and C2, compared to the composites prepared without dispersants. Good electrochemical performance was achieved at a high active mass loading, which was of 30 mg cm^{-2}. Composites C1 and C2 showed capacitances of 4.5 and 4.4 F cm^{-2}, respectively, at a scan rate of 2 mV s^{-1}. However, composite C2 showed a higher capacitance retention at high scan rates, which was found to be 66% at a scan rate of 100 mV s^{-1}. The asymmetric devices, prepared using composite C2 showed promising performance in a voltage window of 1.6 V.

Acknowledgements

The authors gratefully acknowledge the Natural Sciences and Engineering Research Council of Canada for the financial support and Vale Canada for the donation of Ni foam.

Electronic supplementary material: The online version of this article (doi:10.1007/s10853-016-0711-0) contains supplementary material, which is available to authorized users.

References

[1] Devaraj S, Munichandraiah N (2005) High capacitance of electrodeposited MnO_2 by the effect of a surface-active agent. Electrochem Solid State Lett 8:A373–A377

[2] Athouel L, Moser F, Dugas R, Crosnier O, Bélanger D, Brousse T (2008) Variation of the MnO_2 birnessite structure upon charge/discharge in an electrochemical supercapacitor electrode in aqueous Na_2SO_4 electrolyte. J Phys Chem C 112:7270–7277

[3] Bélanger D, Brousse T, Long JW (2008) Manganese oxides: battery materials make the leap to electrochemical capacitors. Electrochem Soc Interface 17:49–52

[4] Li J, Zhitomirsky I (2009) Electrophoretic deposition of manganese dioxide-carbon nanotube composites. J Mater Process Technol 209:3452–3459

[5] Cao J, Li X, Wang Y, Walsh FC, Ouyang J-H, Jia D et al (2015) Materials and fabrication of electrode scaffolds for deposition of MnO_2 and their true performance in supercapacitors. J Power Sources 293:657–674

[6] Wang Y, Liu Y, Zhitomirsky I (2013) Surface modification of MnO_2 and carbon nanotubes using organic dyes for nanotechnology of electrochemical supercapacitors. J Mater Chem A 1:12519–12526

[7] Brousse T, Taberna P-L, Crosnier O, Dugas R, Guillemet P, Scudeller Y et al (2007) Long-term cycling behavior of asymmetric activated carbon/MnO_2 aqueous electrochemical supercapacitor. J Power Sources 173:633–641

[8] Jiang R, Huang T, Tang Y, Liu J, Xue L, Zhuang J et al (2009) Factors influencing MnO_2/multi-walled carbon nanotubes composite's electrochemical performance as supercapacitor electrode. Electrochim Acta 54:7173–7179

[9] Wang Y, Zhitomirsky I (2011) Cathodic electrodeposition of Ag-doped manganese dioxide films for electrodes of electrochemical supercapacitors. Mater Lett 65:1759–1761

[10] Toupin M, Brousse T, Belanger D (2004) Charge storage mechanism of MnO_2 electrode used in aqueous electrochemical capacitor. Chem Mater 16:3184–3190

[11] Nam K-W, Kim K-B (2006) Manganese oxide film electrodes prepared by electrostatic spray deposition for electrochemical capacitors. J Electrochem Soc 153:A81–A88

[12] Xia H, Huo C (2011) Electrochemical properties of MnO_2/CNT nanocomposite in neutral aqueous electrolyte as cathode material for asymmetric supercapacitors. Int J Smart Nano Mater 2:283–291

[13] Gogotsi Y, Simon P (2011) True performance metrics in electrochemical energy storage. Science 334:917–918

[14] Bordjiba T, Belanger D (2010) Development of new nanocomposite based on nanosized-manganese oxide and carbon nanotubes for high performance electrochemical capacitors. Electrochim Acta 55:3428–3433

[15] Yan J, Fan Z, Wei T, Cheng J, Shao B, Wang K et al (2009) Carbon nanotube/MnO_2 composites synthesized by microwave-assisted method for supercapacitors with high power and energy densities. J Power Sources 194:1202–1207

[16] Li Y, Cao D, Wang Y, Yang S, Zhang D, Ye K et al (2015) Hydrothermal deposition of manganese dioxide nanosheets on electrodeposited graphene covered nickel foam as a high-performance electrode for supercapacitors. J Power Sources 279:138–145

[17] Kong S, Cheng K, Gao Y, Ouyang T, Ye K, Wang G et al (2016) A novel three-dimensional manganese dioxide electrode for high performance supercapacitors. J Power Sources 308:141–148

[18] Zhao X, Zhang L, Murali S, Stoller MD, Zhang Q, Zhu Y et al (2012) Incorporation of manganese dioxide within ultraporous activated graphene for high-performance electrochemical capacitors. ACS Nano 6:5404–5412

[19] Zhang C, Zhu X, Wang Z, Sun P, Ren Y, Zhu J et al (2014) Facile synthesis and strongly microstructure-dependent electrochemical properties of graphene/manganese dioxide composites for supercapacitors. Nanoscale Res Lett 9:1–8

[20] Liu Y, Yan D, Zhuo R, Li S, Wu Z, Wang J et al (2013) Design, hydrothermal synthesis and electrochemical properties of porous birnessite-type manganese dioxide nanosheets on graphene as a hybrid material for supercapacitors. J Power Sources 242:78–85

[21] Song H, Li X, Zhang Y, Wang H, Li H, Huang J (2014) A nanocomposite of needle-like MnO_2 nanowires arrays sandwiched between graphene nanosheets for supercapacitors. Ceram Int 40:1251–1255

[22] Ji C, Ren H, Yang S (2015) Control of manganese dioxide crystallographic structure in the redox reaction between graphene and permanganate ions and their electrochemical performance. RSC Adv 5:21978–21987

[23] Shen J, Liu A, Tu Y, Wang H, Jiang R, Ouyang J et al (2012) Asymmetric deposition of manganese oxide in single walled carbon nanotube films as electrodes for flexible high frequency response electrochemical capacitors. Electrochim Acta 78:122–132

[24] Jacob GM, Zhitomirsky I (2008) Microstructure and properties of manganese dioxide films prepared by electrodeposition. Appl Surf Sci 254:6671–6676

[25] Wang G, Zhang L, Zhang J (2012) A review of electrode materials for electrochemical supercapacitors. Chem Soc Rev 41:797–828

[26] Wei W, Cui X, Chen W, Ivey DG (2011) Manganese oxide-based materials as electrochemical supercapacitor electrodes. Chem Soc Rev 40:1697–1721

[27] Ata M, Liu Y, Zhitomirsky I (2014) A review of new methods of surface chemical modification, dispersion and electrophoretic deposition of metal oxide particles. RSC Adv 4:22716–22732

[28] Lin S, Blankschtein D (2010) Role of the bile salt surfactant sodium cholate in enhancing the aqueous dispersion stability of single-walled carbon nanotubes: a molecular dynamics simulation study. J Phys Chem B 114:15616–15625

[29] Wenseleers W, Vlasov II, Goovaerts E, Obraztsova ED, Lobach AS, Bouwen A (2004) Efficient isolation and solubilization of pristine single-walled nanotubes in bile salt micelles. Adv Funct Mater 14:1105–1112

[30] Arnold MS, Green AA, Hulvat JF, Stupp SI, Hersam MC (2006) Sorting carbon nanotubes by electronic structure using density differentiation. Nat Nanotechnol 1:60–65

[31] Ata M, Zhitomirsky I (2015) Colloidal methods for the fabrication of carbon nanotube-manganese dioxide and carbon nanotube-polypyrrole composites using bile acids. J Colloid Interface Sci 454:27–34

[32] Cheong M, Zhitomirsky I (2009) Electrophoretic deposition of manganese oxide films. Surf Eng 25:346–352

[33] Taberna P, Simon P, Fauvarque JF (2003) Electrochemical characteristics and impedance spectroscopy studies of carbon-carbon supercapacitors. J Electrochem Soc 150:A292–A300

[34] Liu Y, Zhitomirsky I (2014) Aqueous electrostatic dispersion and heterocoagulation of multiwalled carbon nanotubes and manganese dioxide for the fabrication of supercapacitor electrodes and devices. RSC Adv 4:45481–45489

[35] Buoro RM, Diculescu VC, Lopes IC, Serrano SH, Oliveira-Brett AM (2014) Electrochemical oxidation of sulfasalazine at a glassy carbon electrode. Electroanalysis 26:924–930

[36] Liu Y, Shi K, Zhitomirsky I (2014) New colloidal route for electrostatic assembly of oxide nanoparticle-carbon nanotube composites. Colloids Surf A 446:15–22

[37] Ata MS, Zhu GZ, Botton GA, Zhitomirsky I (2014) Electrophoretic deposition of manganese dioxide films using new dispersing agents. Adv Appl Ceram 113:22–27

[38] Dobson KD, McQuillan AJ (2000) In situ infrared spectroscopic analysis of the adsorption of aromatic carboxylic acids to TiO_2, ZrO_2, Al_2O_3, and Ta_2O_5 from aqueous solutions. Spectrochim Acta A 56:557–565

[39] Kötz R, Carlen M (2000) Principles and applications of electrochemical capacitors. Electrochim Acta 45:2483–2498

[40] Li X, Zhitomirsky I (2013) Electrodeposition of polypyrrole-carbon nanotube composites for electrochemical supercapacitors. J Power Sources 221:49–56

[41] Su Y, Zhitomirsky I (2013) Cataphoretic assembly of cationic dyes and deposition of carbon nanotube and graphene films. J Colloid Interface Sci 399:46–53

[42] Su Y, Zhitomirsky I (2013) Electrophoretic deposition of graphene, carbon nanotubes and composite films using methyl violet dye as a dispersing agent. Colloids Surf A 436:97–103

[43] Zhu Y, Shi K, Zhitomirsky I (2014) Anionic dopant-dispersants for synthesis of polypyrrole coated carbon nanotubes and fabrication of supercapacitor electrodes with high active mass loading. J Mater Chem A 2:14666–14673

[44] Puchtler H, Meloan SN, Waldrop FS (1979) Aldehyde-fuchsin: historical and chemical considerations. Histochemistry 60:113–123

[45] Ortman R, Forbes W, Balasubramanian A (1966) Concerning the staining properties of aldehyde basic fuchsin. J Histochem Cytochem 14:104–111

[46] Mander ST, Mander L, Carmichael G (1968) The staining mechanism of aldehyde-fuchsin, with reference to the oxytalan fiber in the mouse. J Histochem Cytochem 16:480–485

[47] Yang X, Shi K, Zhitomirsky I, Cranston ED (2015) Cellulose nanocrystal aerogels as universal 3D lightweight substrates for supercapacitor materials. Adv Mater 27:6104–6109

[48] Yang X, Cranston ED (2014) Chemically cross-linked cellulose nanocrystal aerogels with shape recovery and superabsorbent properties. Chem Mater 26:6016–6025

[49] Yu Y, Wang Q, Yuan J, Fan X, Wang P, Cui L (2016) Hydrophobic modification of cotton fabric with octadecylamine via laccase/TEMPO mediated grafting. Carbohydr Polym 137:549–555

[50] Lagadic IL (2006) Schiff base chelate-functionalized organoclays. Microporous Mesoporous Mater 95:226–233

[51] Halder S, Dey S, Roy P (2015) A quinoline based Schiff-base compound as pH sensor. RSC Adv 5:54873–54881

[52] Jankovic IA, Saponjic ZV, Comor MI, Nedeljkovic JM (2009) Surface modification of colloidal TiO_2 nanoparticles with bidentate benzene derivatives. J Phys Chem C 113:12645–12652

[53] Jayaweera PM, Jayarathne TAU (2006) Acid/base induced linkage isomerization of alizarin red adsorbed onto nanoporous TiO_2 surfaces. Surf Sci 600:L297–L300

[54] Gulley-Stahl H, Hogan PA, Schmidt WL, Wall SJ, Buhrlage A, Bullen HA (2010) Surface complexation of catechol to metal oxides: an ATR-FTIR, adsorption, and dissolution study. Environ Sci Technol 44:4116–4121